CrossMark

Partitioning Eddy-Covariance Methane Fluxes from a Shallow Lake into Diffusive and Ebullitive Fluxes

Hiroki Iwata[1] (ORCID) **· Ryuichi Hirata[2] · Yoshiyuki Takahashi[2] · Yuichi Miyabara[3] · Masayuki Itoh[4] · Kotaro Iizuka[5]**

Abstract

Methane (CH_4) is known to be emitted from lakes to the atmosphere via processes such as diffusion and ebullition (i.e., bubble emission). We developed a practical method for partitioning eddy-covariance CH_4 fluxes from a shallow lake into diffusive and ebullitive fluxes using a wavelet analysis based on local scalar similarity between the CH_4 concentration and other reference scalars, such as the air temperature or water vapour concentration, in the wavelet time-scale domain, with the hypothesis that similar and dissimilar fluctuation components are related to diffusive and ebullitive CH_4 fluxes, respectively. Our method is applied to approximately two weeks of data obtained at a shallow mid-latitude lake. The partitioned diffusive flux has a physically sound relationship with wind speed, supporting the validity of the method. The ratio of the diffusive flux to the total flux is typically 0.11 with flow from an area of steady bubble emission, but otherwise 0.36. Further validation is required using a larger dataset and data from other lakes. The proposed method can be easily applied to historical data because it requires only 10-Hz data of CH_4 concentration and other reference scalars, along with an empirical parameter.

Keywords CH_4 flux · Ebullition · Gas exchange · Scalar similarity · Wavelet analysis

1 Introduction

Inland bodies of water are an important source of methane (CH_4), which is a potent greenhouse gas. While the global emission of CH_4 from lakes, reservoirs, and rivers has been

---

✉ Hiroki Iwata
hiwata@shinshu-u.ac.jp

[1] Department of Environmental Sciences, Shinshu University, Matsumoto, Japan

[2] Center for Global Environmental Research, National Institute for Environmental Studies, Tsukuba, Japan

[3] Institute of Mountain Science, Shinshu University, Suwa, Japan

[4] Center for Southeast Asian Studies, Kyoto University, Kyoto, Japan

[5] Center for Spatial Information Science, University of Tokyo, Kashiwa, Japan

estimated by, for example, Bastviken et al. (2011), large uncertainty remains due to uncertain lake-area estimates (Wik et al. 2016) and the heterogeneous emission of CH_4 within a lake.

Methane produced in anoxic sediments in lakes is emitted to the atmosphere via three processes: diffusion within the water column, diffusion within plant aerenchyma, and ebullition (i.e., sporadic bubbling). To model CH_4 emissions accurately, all these processes must be represented correctly in ecosystem models (e.g., Tang et al. 2010). Among these emission processes, ebullition is thought to contribute significantly to the total emissions (Bartlett et al. 1988; Keller and Stallard 1994; Bastviken et al. 2004; Walter et al. 2007). However, due to the sporadic nature of ebullition events, it is difficult to determine the spatially-averaged emission rate and its temporal variability using floating chambers or bubble traps.

Recently, eddy-covariance studies of CH_4 emissions from lakes have been conducted by, for example, Eugster et al. (2011), Schubert et al. (2012), and Podgrajsek et al. (2014a, b, 2016). As eddy-covariance observations provide continuous data on the net exchange between the surface and the atmosphere, with spatial coverage on the order of 10^4 m^2, this approach has advantages in terms of spatial coverage and temporal resolution. However, conventional eddy-covariance observations cannot distinguish the processes involved in the net exchange, which is problematic when developing statistical relationships between CH_4 emissions and environmental variables, because each emission process is influenced by different environmental variables. Nonetheless, recent studies (Scanlon and Sahu 2008; Thomas et al. 2008; Kotthaus and Grimmond 2012) have suggested that raw turbulence data preserve information on exchange processes in agricultural and forest ecosystems, and on emissions from specific locations in urban areas, which is useful information for the partitioning of eddy-covariance-derived water vapour (H_2O) and carbon dioxide (CO_2) fluxes. While Schaller et al. (2017) developed a method for CH_4 using a wavelet transform to calculate fluxes during short turbulent events to evaluate temporally local emissions, such as ebullition, to our knowledge no partitioning method has been developed for application to eddy-covariance-derived CH_4 fluxes.

The development of a partitioning method for the eddy-covariance-derived CH_4 flux (hereafter, the CH_4 flux) should help in quantifying CH_4 exchange in individual-site studies, and when scaling up CH_4 exchange to larger areas. As eddy-covariance datasets often contain many gaps due to unsuitable atmospheric conditions for measurement (Vickers and Mahrt 1997) and instrument maintenance, these data gaps must be filled so as to derive the cumulative exchange. Partitioning the CH_4 flux facilitates the development of separate statistical relationships between different CH_4 emission processes and specific environmental variables, which are relationships useful for the filling of gaps in flux data to obtain accurate cumulative emissions. One option for upscaling CH_4 exchange is to use ecosystem models that have been parametrized and validated against CH_4 flux data (e.g., Xu et al. 2016), for which partitioned CH_4 flux data can be used to achieve more accurate parametrizations of the emission processes.

We present a practical method to partition the CH_4 flux recorded over a shallow lake into diffusive and ebullitive fluxes using a wavelet analysis based on local scalar similarity in the wavelet time-scale domain, and requiring only turbulence data of CH_4 concentration and other reference scalars, such as the air temperature, and the H_2O and CO_2 concentrations. The method is applied to observations above a shallow mid-latitude lake, and the environmental controls on partitioned diffusive and ebullitive fluxes are examined.
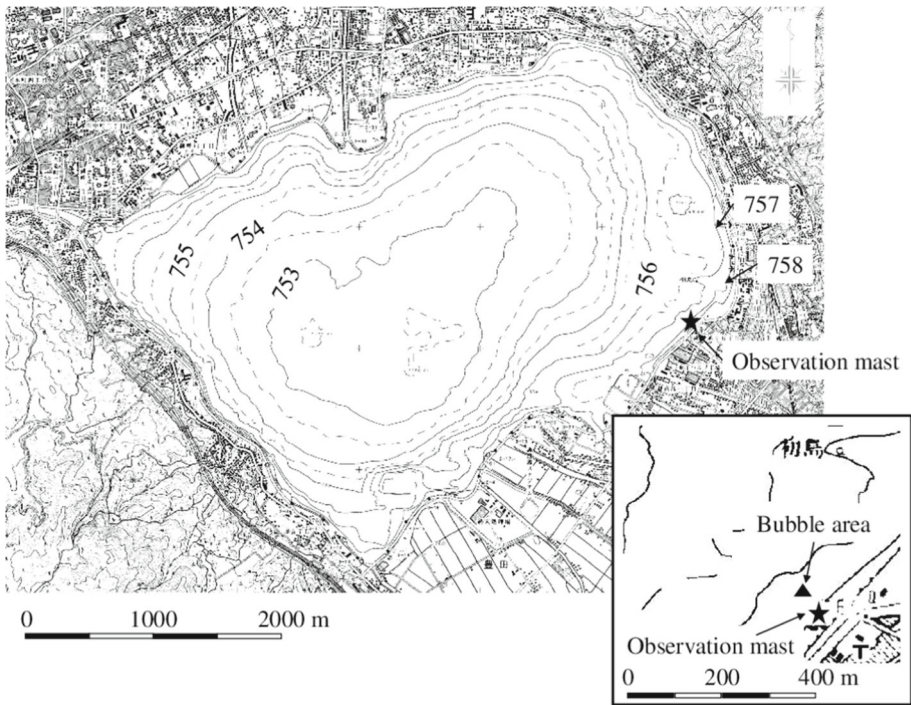
Fig. 1 Bathymetric map of Lake Suwa obtained in 2005. Contours indicate the elevation above sea level, and 758 m approximately corresponds to a water depth of 1.8 m at the time of observation. The location of the observation mast on the south-east shore is indicated with a star. An enlarged view of the area close to the observation mast (lower right) indicates an area with steady CH_4 bubble emissions (triangle)

2 Observation and Data Analyses

2.1 Study Site

Analyzed here are data obtained at Lake Suwa (Fig. 1), which is a shallow eutrophic lake in Nagano, Japan (Park et al. 1998; Ikenaka et al. 2005; Sharma et al. 2016), with a total area of 13.3 km^2, a mean depth of approximately 4 m, and a maximum depth of 6.9 m. Water caltrop (*Trapa japonica* Flerow, a floating-leaved plant) and Esthwaite waterweed (*Hydrilla verticillata* (L.f.) Royle, a submerged plant) grow along the lake shores during summer, although there were no emergent macrophytes near the observation site. The prevailing wind direction for this site is between west-north-west and north-west.

Steady CH_4 bubble emissions occur in certain areas at Lake Suwa (Nakamura and Owa 1952), one of which we found at a distance of 55 m in a direction of 325° from the observation mast (Fig. 1). Bubbles were collected underwater every three months in 2017, and were analyzed with a gas chromatograph, indicating a CH_4 volume concentration of 85–88%, with no obvious seasonal variation.

2.2 Observations

An eddy-covariance system was installed on a pier (36° 2′ 47.66″N, 138° 6′ 30.07″E) on the south-east shore, consisting of an ultrasonic anemo–thermometer (CSAT3, Camp-

bell Scientific, Logan, Utah, USA), open-path CH_4 analyzer (LI-7700, Li-Cor, Lincoln, Nebraska, USA), open-path CO_2/H_2O analyzer (EC-150, Campbell Scientific), and data logger (CR3000, Campbell Scientific). The observation height varied depending on the water level, but was approximately 3.2 m throughout the observation period. The sensor separation from the ultrasonic anemo–thermometer was 0.25 m for the CH_4 analyzer and 0.05 m for the CO_2/H_2O analyzer. Turbulence data were recorded at 10 Hz. Relevant atmospheric and lake water observations were also collected, including the wind speed, air pressure (PTB110, Vaisala, Finland), the water-temperature profile (107, Campbell Scientific), water level (CS451, Campbell Scientific), and radiation (CNR4, Kipp and Zonen, Delft, The Netherlands), with 30-min averages recorded by the same data logger.

2.3 Data Processing and Selection

Prior to data analysis, spikes were removed from the raw 10-Hz data (Vickers and Mahrt 1997). Data from the two gas analyzers were synchronized with data from the ultrasonic anemo–thermometer to account for lag times due to sensor separations and internal processing using a cross-correlation analysis (Iwata et al. 2014). The 10-Hz data were then corrected point by point (Detto and Katul 2007) for the difference between the sonic virtual temperature and dry-bulb temperature (Schotanus et al. 1983), the air density variation (Webb et al. 1980), and spectroscopic effect (McDermitt et al. 2011).

We analyzed data obtained in mid-summer (17–31 August) of 2016, with the distribution of wind directions during this period shown in Fig. 2. Because the observation mast was located near the shore, the analysis was confined to data collected for flow from the lake, corresponding to 223°–033°. For this sector, the flux footprint calculated using the model of Kormann and Meixner (2001) is typically 300–500 m, but less than 1000 m in length for most cases. The raw 10-Hz data were visually inspected, with data collected during rain events and instrument malfunction discarded. The 30-min data were also filtered using a stationarity index (Mahrt 1998), with strongly non-stationary data removed from the analysis, leaving 145 30-min records. The mean and standard deviation of each flux are 0.02 ± 0.01 K m s^{-1}, 2.57 ± 1.32 mmol m^{-2} s^{-1}, -0.41 ± 1.21 μmol m^{-2} s^{-1}, and 0.39 ± 0.29 μmol m^{-2} s^{-1} for

Fig. 2 Distribution of wind directions during the analysis period. Solid and dashed lines represent daytime and night-time, respectively
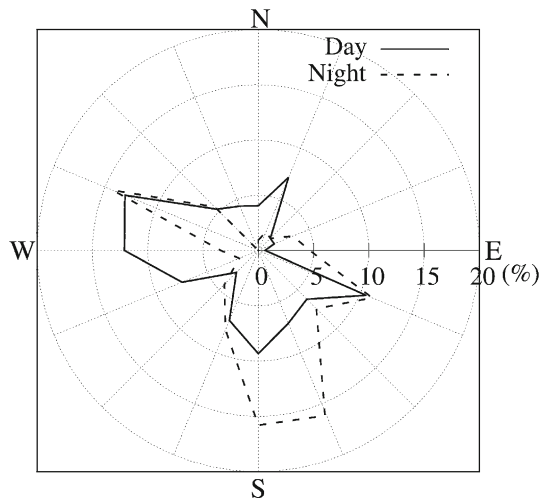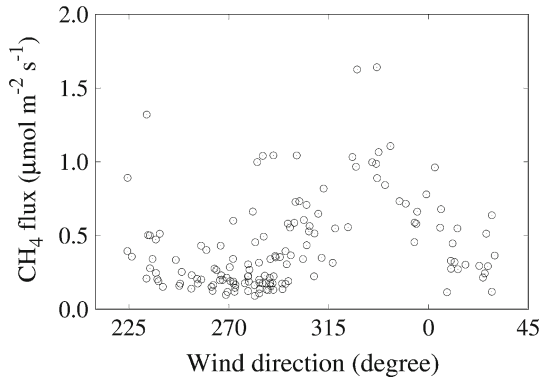
Fig. 3 Dependence of CH_4 flux on wind direction

the temperature, H_2O, CO_2, and CH_4, respectively. Time series of these fluxes during the observation period are shown in Fig. S1 (Supplementary Material). Figure 3 shows the wind-direction dependence of the CH_4 flux for the observation period, indicating larger fluxes for flow from the area with steady CH_4 bubble emissions.

3 Results and Discussion

3.1 Development of the Partitioning Methodology

The water surface is flat and homogeneously illuminated by shortwave radiation, such that the source distributions of sensible heat and water vapour can be assumed to be spatially quasi-homogeneous, at least within the flux footprint for instruments mounted a few metres above the water surface. The source distributions of the gases that diffused into the atmosphere are also spatially quasi-homogeneous because dissolved gases mix within the water column. These scalars emitted into the atmosphere are transported by the same eddies and sensed by instruments at a single point in the atmosphere, leading to similar turbulent fluctuations among scalars. However, ebullition events lack spatial homogeneity in the source distribution of CH_4 because ebullition occurs heterogeneously in both space and time, leading to scalar dissimilarity of the turbulent fluctuations observed in the atmosphere (Katul et al. 1995). Therefore, we hypothesized that the turbulent fluctuations of the CH_4 concentration similar to those of the air temperature, H_2O concentration, or CO_2 concentration are related to the diffusion process of CH_4 transfer, while dissimilar turbulent fluctuations in the CH_4 concentration are related to the ebullition process. Consequently, the recorded turbulent fluctuation in the CH_4 concentration is then the superposition of those fluctuations related to the two processes. As there were no emergent macrophytes within the flux footprint, we neglected the contribution from plant-mediated transport. Also, since non-local processes, such as entrainment or advection, may influence scalar similarity (De Bruin et al. 1993, 1999; Detto et al. 2008), we evaluated the degree of influence from these non-local processes for each scalar in the flux–variance relationship, as described below.

Figure 4 shows typical examples of high-frequency turbulent fluctuations of air temperature (T), H_2O density (q), CO_2 density (c), and CH_4 density (m) for cases with low and high CH_4 emissions. To show the degree of similarity between scalars, we calculated wavelet coherences (Scanlon and Albertson 2001) around the spectral peak frequencies, and obtained values of 0.98, -0.80, 0.92, -0.85, 0.92, and -0.78 for the T–q, T–c, T–m, q–c, q–m, and
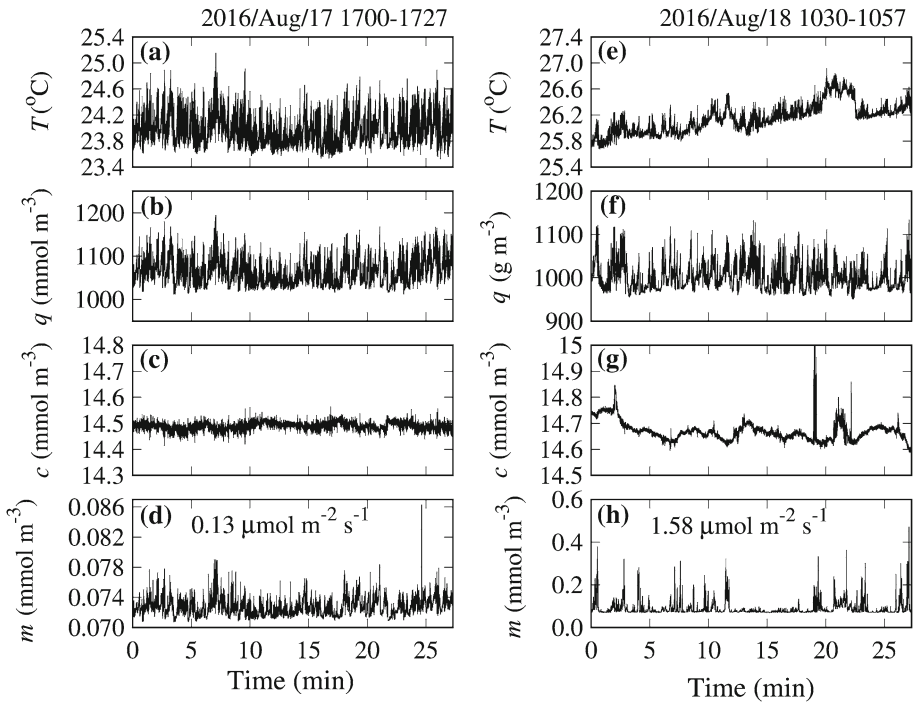
Fig. 4 Typical 10-Hz data for **a**, **e** air temperature (T), **b**, **f** H_2O density (q), **c**, **g** CO_2 density (c), and **d**, **h** CH_4 density (m) for 27-min data with low CH_4 fluxes (left, observed from 1700–1727 on 17 August 2016) and high CH_4 fluxes (right, observed from 1030–1057 on 18 August 2016). The values for the CH_4 flux for each case are indicated in each panel. Note that the range of the *y*-axis for the CH_4 density differs between the two cases

c–m coherences, respectively, for the case with a low CH_4 flux (Fig. 4a–d), implying similar fluctuations of the four scalars for low values of the CH_4 flux. The correlations including CO_2 are lowest because the small flux relative to the atmospheric concentration leads to lower turbulent fluctuations (Fig. 4c and Fig. S1c). The corresponding wavelet coherences for the case with a high CH_4 flux (Fig. 4e–h) are 0.80, −0.08, 0.50, −0.09, 0.53, and −0.02 for T–q, T–c, T–m, q–c, q–m, and c–m, respectively, indicating that, although the air temperature and H_2O density values are similar (Fig. 4e, f), the fluctuation in CH_4 density is dissimilar to those of the three other scalars on account of large positive deviations from the average (Fig. 4h) resulting from ebullition events. At this site, data indicating such ebullition events were the norm rather than the exception, occurring during approximately 80% of the observation period as identified by visual inspection of 10-Hz data, despite a variation in the intensity of ebullition and its frequency within the 30-min period. Larger-scale fluctuations are evident in the CO_2 density time series data (Fig. 4g), resulting in almost negligible correlations with other scalars.

Figure 5 shows the dependence of selected scalar–scalar correlations on the wind direction. The correlation coefficient between the H_2O density and CH_4 density is lower for flow from the steady bubble emission area (wind direction class 5) and the neighbouring area, and generally higher as the flow veered away from the steady bubble emission area. The correlation coefficient between the air temperature and H_2O density is reduced as the flow veers towards the shore (wind direction classes 1 and 8), which may reflect the influence
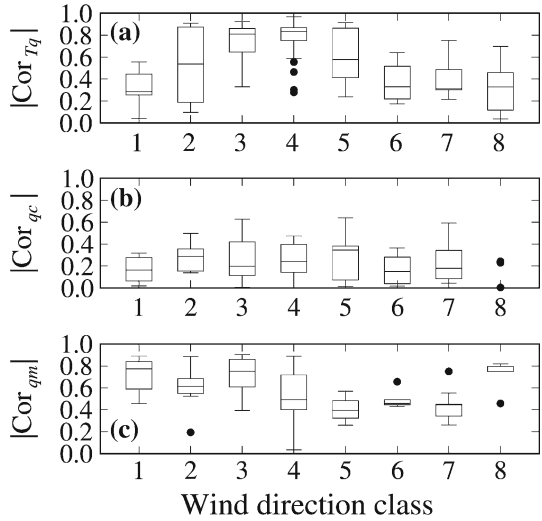
of non-local processes. Other scalar–scalar correlations show qualitatively similar results (Fig. S2 in the Supplementary Material). Because the magnitudes of the CO_2 flux (Fig. S1c) and its correlation with other scalars (Fig. 5b) are generally small, we omit the results related to CO_2 hereafter.

To further show the general effects of ebullition on the turbulent fluctuations, the wavelet variance, wavelet covariance, and wavelet coherence for all 30-min records are presented in Fig. 6, showing only data with a sufficient flux magnitude (see the caption for further details). In the wavelet variance spectra (Fig. 6a, b), the H_2O density and CH_4 density had similar spectral curves, with the CH_4 variance peak occurring at a slightly higher frequency than the H_2O variance peak; the CH_4 variance is also slightly more scattered than the H_2O variance around the spectral peak. The wavelet covariance spectra (Fig. 6c, d) also shows a similar cospectral curve between the vertical velocity component (w)–H_2O covariance and the w–CH_4 covariance, which is again slightly more scattered around the spectral peak. The wavelet variance of air temperature and covariance between the vertical velocity component and air temperature exhibit similar curves to those shown in Fig. 6 (data not shown). Thus, the effect of ebullition on the wavelet variance and covariance spectra is ambiguous, although ebullition occurred frequently at this site, because the time scale of ebullition is close to that of the spectral peak for general surface-layer turbulence. In contrast, the effect of ebullition on wavelet coherence is evident (Fig. 6e, f). Although most coherence between the air temperature and H_2O density around the spectral peak is close to unity, the coherence between the H_2O density and CH_4 density has a wider distribution, ranging from 0.3 to 1 around the spectral peak, implying the occurrence of ebullition results in scalar dissimilarity. The coherence is low at the higher end of the frequency range ($z_{obs}/j\overline{u} > 1$, where z_{obs} is the observation height above the water surface (m), j is the time scale (s), and $\overline{u}$ is the average longitudinal wind speed (m s^{-1})) due to the sensor separation and the smaller turbulent eddy scale, while there is more scatter at the lower end of the frequency range ($z_{obs}/j\overline{u} < 10^{-2}$) due to the possible influence of entrainment (Asanuma et al. 2007) and large-scale advection (Saito et al. 2007).

To partition the contributions from diffusion and ebullition processes, scalar similarity was examined in the wavelet time-scale domain. Wavelet coefficients (i.e., data in the time-scale
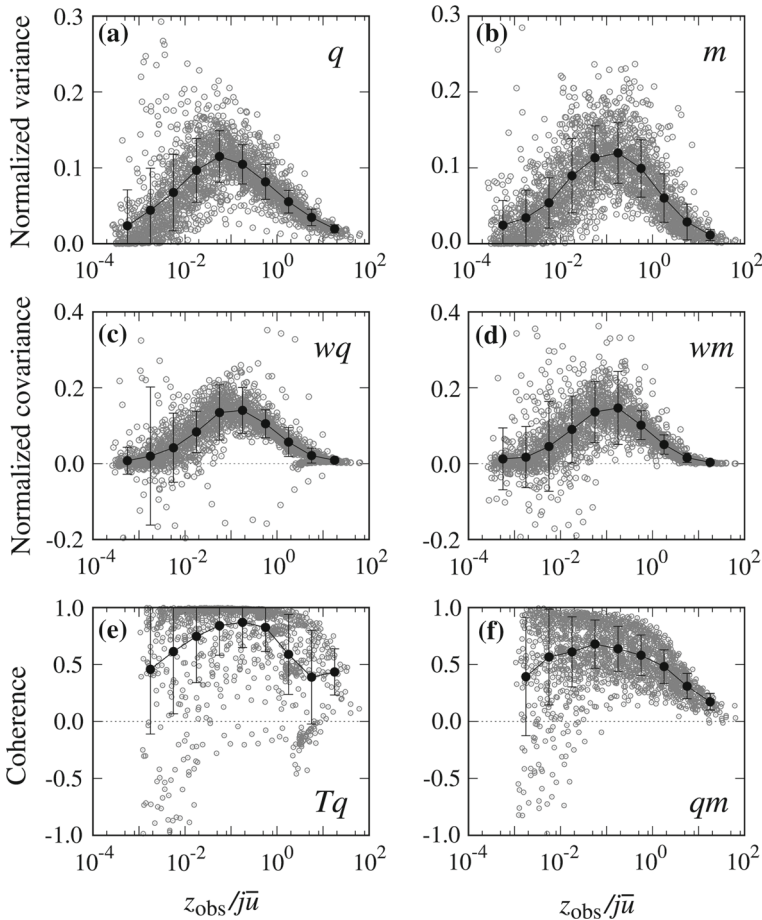
Fig. 6 Normalized wavelet variance spectra for **a** H_2O density (q) and **b** CH_4 density (m); normalized wavelet covariance spectra **c** between the vertical velocity component (w) and H_2O density, and **d** between the vertical velocity component and CH_4 density; the wavelet coherence **e** between the temperature (T) and H_2O density and **f** between the H_2O density and CH_4 density. The x-axis is a time scale (j) normalized by the observation height (z_{obs}) and the average longitudinal wind speed ($\overline{u}$). Black solid circles and error bars indicate bin averages and standard deviations, respectively. Small values $|\overline{w'T'}| < 0.01$ K m s^{-1}, $|\overline{w'q'}| < 0.05$ mmol m^{-2} s^{-1}, and $|\overline{w'm'}| < 0.1$ μmol m^{-2} s^{-1} have been removed for presentation purposes (here, the bar and prime indicating time averaging and a deviation, respectively), leaving 93, 143 and 143 30-min data points for the panels corresponding to T, q and m, respectively

domain) of variable x (W_x) were calculated based on the Haar mother wavelet using the orthonormal wavelet transform (Kumar and Foufoula-Georgiou 1994; Percival and Walden 2000),

$$W_x^{j,i} = \int_{-\infty}^{\infty} x(t) \psi_{j,i}(t) \mathrm{d}t, \tag{1}$$

where i is the time location, t is time, and $\psi_{j,i}(t) = 2^{-j/2} \psi(2^{-j}t - i)$ with ψ as the mother wavelet function. The variable can be the vertical velocity component (w), air temperature (T), H_2O density (q), or CH_4 density (m). We compared the converted wavelet coefficients
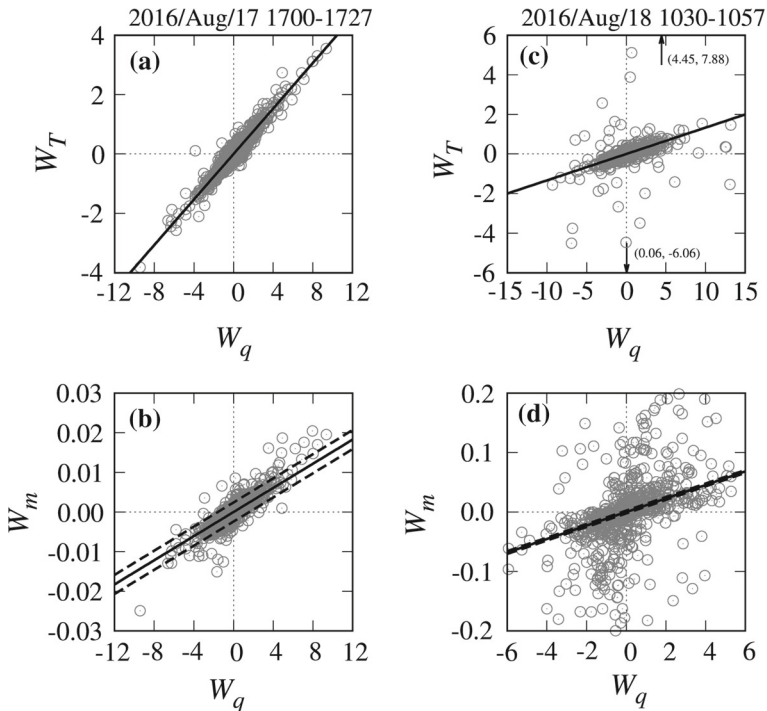
Fig. 7 Comparisons of **a, c** wavelet coefficients between air temperature (W_T) and H_2O density (W_q), and **b, d** wavelet coefficients between H_2O density (W_q) and CH_4 density (W_m) for cases with low (left) and high (right) CH_4 flux calculated from the 10-Hz data shown in Fig. 4. Numbers and arrows in the upper right panel indicate that two data points exist beyond the panel. The lower right panel shows only the centremost part of the figure, and many data points exist beyond the panel. Straight lines are determined using the iteratively-reweighted least-squares method

among scalars for the same scale and same time location in a scatter plot (Fig 7). Here, coefficients for a selected range of the normalized time scale, namely $0.003 < z_{\mathrm{obs}}/j\bar{u} < 1$, were used for comparisons because the coefficients of these scales explained most of the covariances (Fig. 6d) and smaller and larger scales do not necessarily retain scalar similarity (Fig. 6f). We refer to the scales of the selected range as flux-transporting eddy scales. If the similarity between two scalars holds, the wavelet coefficient distribution should collapse onto a straight line, which is apparent in the comparison of W_T and W_q in both cases (Fig. 7a, c) and the comparison of W_q and W_m in the case with low CH_4 flux (Fig. 7b). For the case with high CH_4 flux, the comparison of W_q and W_m values shows extremely large scatter (Fig. 7d). Some coefficients, however, appear to distribute around a straight line, indicating that turbulent fluctuations of the CH_4 density are a mixture of similar and dissimilar fluctuations, which correspond to diffusive and ebullitive emission processes, respectively.

Coefficients due to diffusion and ebullition processes were separated in the following manner. A straight line was first determined as in Fig. 7 using the iteratively-reweighted least-squares method (Rousseeuw and Leroy 2003) with the *MASS* package in the R statistical software (Ripley et al. 2017), then the coefficients for CH_4 density were separated into two groups according to their deviation from the straight line. The group of coefficients located within and outside a certain bound (dashed lines in Fig. 7b and d) is related to diffusive and

ebullitive emission, respectively, where ebullition refers to both sporadic and steady bubble emission. The bound was determined empirically as the typical root-mean-square deviation from the straight line based on several 30-min data without apparent ebullition (Fig. 7b is one example) multiplied by a factor of three. Assuming the deviations from the line are normally distributed, then 99.7 % of deviations are within the bound. This separation was applied not only to the flux-transporting eddy scales but also to the smaller scales.

The procedure described above was applied to all 30-min data, and the diffusive flux was calculated from W_w and W_m for the 30-min data as

$$F_{\text{diff}} = \frac{1}{N} \sum_{j < z_{\text{obs}}/0.003\overline{u}} \sum_i W_w^{j,i} W_c^{j,i} \delta^{j,i}, \qquad (2)$$

where N is the number of data points, and $\delta^{j,i}$ is an indicator function for the separation of coefficients, defined as unity when W_m is inside the bound, and as zero otherwise. The ebullitive flux was similarly calculated as Eq. 2 with $\delta^{j,i}$ defined as unity when W_m is outside the bound, and as zero otherwise. Transport occurring at $j > z_{\text{obs}}/0.003\overline{u}$ was treated separately, and was not added to either the diffusive or the ebullitive flux, with the contribution from this large-scale fluctuation to the diffusive flux negligible, affecting ebullitive fluxes only slightly when included in the partitioning procedure. In addition, as the time scale of ebullition is usually less than a few minutes, the contribution from $j > z_{\text{obs}}/0.003\overline{u}$ was not included in the calculation of the ebullitive flux.

The partitioning method requires a correct choice of the reference scalar to which the CH$_4$ wavelet coefficients are compared. Because non-local processes can also affect the scalar similarity, wavelet coefficients may be found outside the bound in the scatter plot and mistakenly identified as ebullition when such non-local processes affect the fluctuation of the reference scalar. The degree of influence from non-local processes is investigated in the flux–variance relationship (De Bruin et al. 1993; van de Boer et al. 2014) in Fig. 8. Whereas most H$_2$O variance data closely follows the universal function, the air-temperature variance exhibits more scatter deviating from the universal function regardless of the wind direction, which suggests that the air-temperature fluctuation is affected to a greater degree by non-local processes at this site. Therefore, the H$_2$O density was chosen as the most appropriate reference scalar, but we removed 15 data points that deviated from the universal function of the H$_2$O
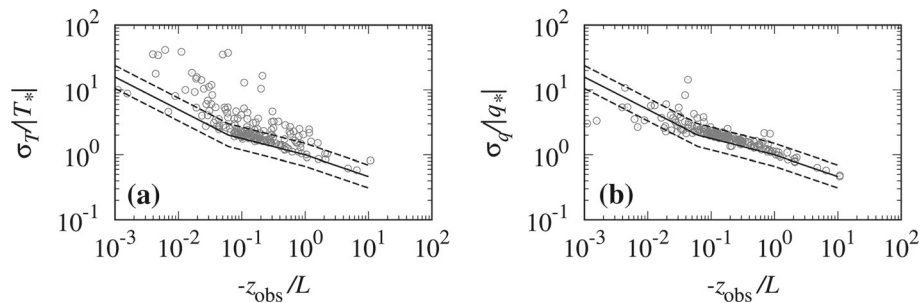

Fig. 8 Dependence of normalized variance on atmospheric stability for **a** temperature and **b** H$_2$O density. Here, T_* and q_* are the temperature and H$_2$O scales defined as $-\overline{w'T'}/u_*$ and $-\overline{w'q'}/u_*$, respectively, where u_* is the friction velocity. The atmospheric stability is defined as z_{obs}/L, where L is the Obukhov length. Solid lines represent the universal function for temperature (ϕ_T) derived in Foken (2008), and dashed lines represent $1.5\phi_T$ and $\phi_T/1.5$. Only data with $z_{\text{obs}}/L < 0$ are shown, as there were only five data points with $z_{\text{obs}}/L > 0$

density (outside the dashed lines in Fig. 8b) from further analysis due to the possible influence of non-local processes.

3.2 Application and Evaluation

We applied this method to data obtained for a 15-day period (17–31 August 2016) at Lake Suwa, and examined the dependence of the CH_4 flux on the environmental variables (Fig. 9). Flux data with flow from both the steady bubble emitting area and other areas were used, unless otherwise stated. First, it is clear that a reasonable relationship between the total CH_4 flux and either the lake bottom water temperature or wind speed does not exist as expected (Fig. 9a, c), stemming in part from characteristics of the eddy-covariance-derived flux data, which represent the total emissions, including both diffusion and ebullition processes. As the total emission is larger for flow from the steady bubble emitting area (Fig. 3), it is difficult to relate the total flux to a single environmental variable. In comparison, the partitioned diffusive CH_4 flux is distributed close to the lower boundary of the total fluxes, and is more predictable from a single environmental variable. There is no detectable difference between partitioned diffusive fluxes for flow from the steady bubble emitting area and those from the other areas (Fig. 9b, d). In addition, the partitioned diffusive CH_4 flux appears dependent on the wind speed (Fig. 9d) rather than the lake bottom water temperature (Fig. 9b), implying that the short-term variation in diffusive emission is controlled by the transport efficiency both at the air–water interface and within the water column rather than by CH_4 production in the lake sediments. This result is reasonable because the gas transfer coefficient at the air–water interface is known to depend on sub-surface turbulence and wind waves, which are controlled by the wind speed (Wanninkhof 1992; Bock et al. 1999; Wanninkhof et al. 2009). Examining the effect of water-side convection on the CH_4 flux using the effective heat flux (Imberger 1985; Podgrajsek et al. 2014b) indicates its effect to be negligible (data not
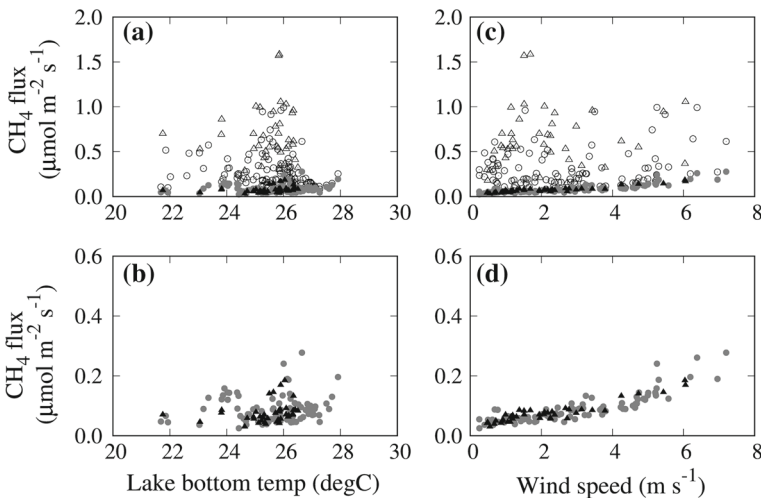

Fig. 9 Dependence of CH_4 flux on lake bottom water temperature (left) and wind speed (right). The upper panels **a**, **c** show both the total flux (open symbols) and partitioned diffusive flux (solid symbols), and the lower panels **b**, **d** show only the partitioned diffusive flux. Data with wind direction from the steady bubble emitting area (295–355°) are indicated by triangles; other data are indicated by circles. Data were obtained from 17 to 31 August 2016

shown). The sediment temperature (for which lake bottom water temperature is a surrogate variable) did not vary markedly during this short period. This physically-sound dependence of the diffusive CH_4 flux on environmental variables supports the validity of our method.

The increase in diffusive CH_4 flux with wind speed is enhanced for wind speeds $> 4 \, \mathrm{m \, s^{-1}}$. The value of the slope fitted to the data is 0.015 for wind speeds $< 4 \, \mathrm{m \, s^{-1}}$, while the slope fitted to data for wind speeds $> 4 \, \mathrm{m \, s^{-1}}$ is 0.05, which may be related to microscale wave breaking (Csanady [1990]; Jessup et al. [1997]; Zappa et al. [2001]) occurring at low to moderate wind speeds (approximately 5–10 $\mathrm{m \, s^{-1}}$). This enhances gas diffusion at the air–water interface by disturbing the thin diffusive water layer, and thereby increasing the concentration differences between the atmosphere and surface water layer.

The ratio of diffusive flux to total flux for $j < z_{\mathrm{obs}}/0.003\overline{u}$ is 0.05–0.50, with a median value of 0.11 for flow from the steady bubble emitting area, and with the corresponding range and median of the ratio for other wind directions 0.07–0.93 and 0.36, respectively.

We also examined the environmental controls of the partitioned ebullitive flux. In this case, data for flow from the steady bubble emitting area are excluded to determine the environmental controls on sporadic bubble emissions. However, no clear relationships with environmental variables are found. There are slight non-significant decreasing trends with increasing wind speed, lake bottom water temperature, atmospheric pressure, and water level (data not shown). As ebullition is triggered by either shear stress on the sediment surface (Joyce and Jewell [2003]) or a decrease in atmospheric pressure and water level (Martens and Klump [1980]; Mattson and Likens [1990]; Boles et al. [2001]; Tokida et al. [2005]; Varadharajan and Hemond [2012]), we may need to choose an appropriate time scale at which to analyze the environmental controls, as well as to consider the accumulation process. We will further evaluate the environmental controls of ebullition in the future using a larger dataset.

The above examination validates the proposed flux-partitioning method, at least in a qualitative sense. A further quantitative comparison was conducted by estimating the diffusive CH_4 flux using a gas-transfer velocity model proposed by McGillis et al. ([2004]), which Heiskanen et al. ([2014]) reported reproduces the observed gas-transfer velocity well for a stratified lake. A range of surface-dissolved CH_4 concentrations (0.61–1.99 $\mu\mathrm{mol \, L^{-1}}$) observed a few times during the summer of 2016 was used to calculate the concentration difference. The dissolved CH_4 concentration was analyzed with a gas chromatograph using the head-space method. The estimated diffusive fluxes ranged from 0.02 to 0.06 $\mu\mathrm{mol \, m^{-2} \, s^{-1}}$ at a wind speed of 4 $\mathrm{m \, s^{-1}}$ for the range of dissolved concentrations. The partitioned diffusive CH_4 flux from the eddy-covariance observations ranged from approximately 0.07 to 0.13 $\mu\mathrm{mol \, m^{-2} \, s^{-1}}$ at a wind speed of 4 $\mathrm{m \, s^{-1}}$ (Fig. 9d), which is greater than the estimated flux. We do not yet know the reason for this discrepancy, but continuous dissolved CH_4 concentration data may be necessary for a detailed examination.

Partitioned ebullitive fluxes are compared with fluxes calculated using the method of Schaller et al. ([2017]) for continuous data during the period from 930–1230 local time on 18 August 2016 (Fig. 10 and Table 1). Although the fluxes calculated in this manner include contributions from diffusive emission, both fluxes roughly agree.

One limitation of the flux-partitioning method is its application to a much greater observation height. As this height increases, the dilution of high-concentration parcels emitted through ebullition by turbulence proceeds until the parcel reaches the observation height. In this case, turbulent fluctuations caused by ebullition may partly regain scalar similarity, and contributions from ebullition may be underestimated. One necessary improvement is a separation of the effects of ebullition and non-local processes in the turbulent fluctuations. For example, we have excluded the flux contribution from the low-frequency component to minimize the effect from non-local processes, with data possibly influenced by non-local
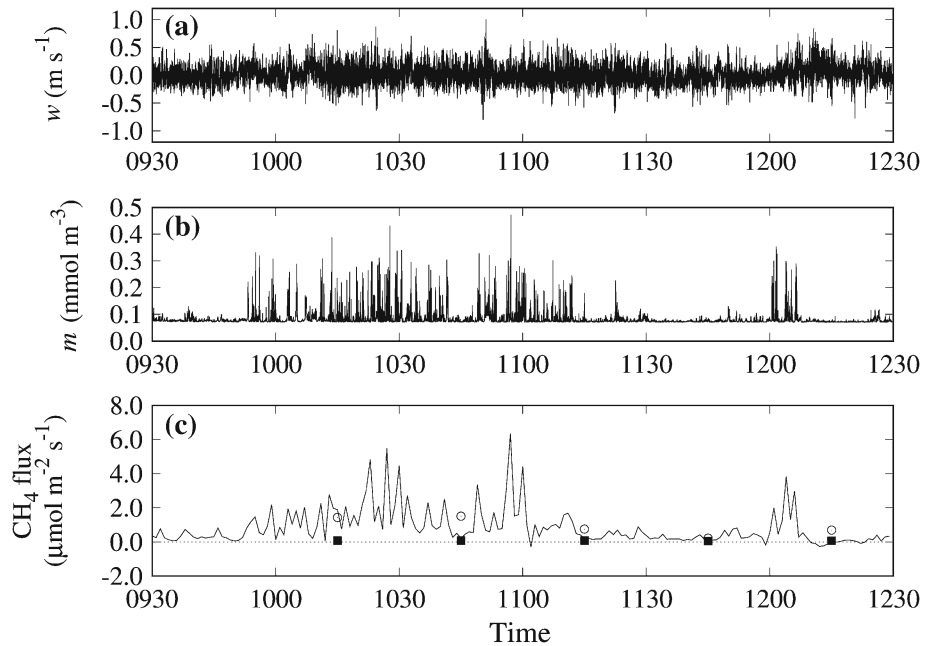
Fig. 10 Time series of **a** the vertical velocity component (w), **b** CH_4 density (m) observed from 930–1230 local time on 18 August 2016, and **c** calculated 1-min averaged CH_4 fluxes using the method of Schaller et al. 2017 (line) and the partitioning method (open circle symbol for the ebullitive flux and solid square for the diffusive flux). The method of Schaller et al. (2017) is applied using the Mexican hat wavelet

Table 1 Partitioned ebullitive fluxes and averaged fluxes calculated following the method of Schaller et al. (2017) for data in Fig. 10

	1000–1030	1030–1100	1100–1130	1130–1200	1200–1230
This study	1.43	1.51	0.75	0.22	0.69
Schaller et al.	1.61($\pm$1.26)	1.48($\pm$1.37)	0.72($\pm$0.83)	0.23($\pm$0.24)	0.48($\pm$0.93)

The unit is μmol m^{-2} s^{-1}. In the Schaller et al. (2017) method, fluxes less than 0.2 μmol m^{-2} s^{-1} are assumed to be the results of diffusive emission, and are replaced with a zero ebullitive flux before averaging to compare with partitioned ebullitive fluxes. This threshold value is determined from the approximate maximum value of the partitioned diffusive flux during the observation period

processes removed from the analysis, but we cannot exclude the possibility that higher frequency components are also affected by non-local processes (e.g., Kimmel et al. 2002). To minimize such effects, it may be better to use a scalar with sufficient surface-flux magnitude such as H_2O density, rather than air temperature or CO_2 density, as performed here. A more thorough understanding of the effect from non-local processes on turbulence could improve the partitioning method. Secondly, to separate contributions from diffusion and ebullition, we use three times the root-mean-square deviation from a fitted straight line as the bounds, but this choice is not based on any physical rationale. We performed a sensitivity test by changing the multiplier to two or four, and found that the magnitude of the diffusive CH_4 flux changed by 10%, indicating that the partitioning result is sensitive to this empirical parameter. While a plausible value may be three, this sensitivity should be borne in mind.

4 Conclusions

We developed a partitioning method for the measured eddy-covariance CH_4 flux from a shallow lake based on a wavelet analysis and the scalar-similarity concept. Ebullition events occur heterogeneously in both space and time, and result in large positive deviations from the temporal average, leading to scalar dissimilarity. These dissimilar components may be separated from similar components in the wavelet time-scale domain, with the calculation of fluxes carried out separately for diffusive and ebullitive emissions. The partitioning method was applied to 15 days of data obtained above a shallow mid-latitude lake. The partitioned diffusive flux shows a physically sound dependence on wind speed, supporting the validity of the method. Note that while these results cannot be obtained for the total CH_4 flux, the partitioning method helps to clarify the basis of CH_4 emissions from lakes. Although the method needs further improvement and validation using a larger dataset and data from other lakes, it is potentially useful because it requires only the turbulent fluctuations of CH_4 density and other scalars, along with an empirical parameter. Therefore, it can be easily applied to data obtained in the past.

References

Asanuma J, Tamagawa I, Ishikawa H, Ma Y, Hayashi T, Qi Y, Wang J (2007) Spectral similarity between scalars at very low frequencies in the unstable atmospheric surface layer over the Tibetan plateau. Boundary-Layer Meteorol 122:85–103

Bartlett KB, Crill PM, Sebacher DI, Harriss RC, Wilson JO, Melack JM (1988) Methane flux from the central Amazonian floodplain. J Geophys Res 93:1571–1582

Bastviken D, Cole J, Pace M, Tranvik L (2004) Methane emissions from lakes: dependence of lake characteristics, two regional assessments, and a global estimate. Global Biogeochem Cycles 18:GB4009. https://doi.org/10.1029/2004GB002238

Bastviken D, Tranvik LJ, Downing JA, Crill PM, Enrich-Prast A (2011) Freshwater methane emissions offset the continental carbon sink. Science 331:50. https://doi.org/10.1126/science.1196808

Bock EJ, Hara T, Frew NM, McGillis WR (1999) Relationship between air-sea gas transfer and short wind waves. J Geophys Res 104:25,821–25,831

Boles JR, Clark JF, Leifer I, Washburn L (2001) Temporal variation in natural methane seep rate due to tides, Coal Oil Point area, California. J Geophys Res 106:27,077–27,086

Csanady GT (1990) The role of breaking wavelets in air-sea gas transfer. J Geophys Res 95:749–759

De Bruin HAR, Kohsiek W, Van den Hurk BJJM (1993) A verification of some methods to determine the fluxes of momentum, sensible heat, and water vapour using standard deviation and structure parameter of scalar meteorological quantities. Boundary-Layer Meteorol 63:231–257

De Bruin HAR, Van den Hurk BJJM, Kroon LJM (1999) On the temperature-humidity correlation and similarity. Boundary-Layer Meteorol 93:453–468

Detto M, Katul GG (2007) Simplified expressions for adjusting higher-order turbulent statistics obtained from open path gas analyzers. Boundary-Layer Meteorol 122:205–216. https://doi.org/10.1007/s10546-006-9105-1

Detto M, Katul GG, Mancini M, Montaldo N, Albertson JD (2008) Surface heterogeneity and its signature in higher-order scalar similarity relationships. Agric For Meteorol 148:902–916. https://doi.org/10.1016/j.agrformet.2007.12.008

Eugster W, DelSontro T, Sobek S (2011) Eddy covariance flux measurements confirm extreme CH_4 emissions from a Swiss hydropower reservoir and resolve their short-term variability. Biogeosciences 8:2815–2831. https://doi.org/10.5194/bg-8-2815-2011

Foken T (2008) Micrometeorology. Springer, Berlin

Heiskanen JJ, Mammarella I, Haapanala S, Pumpanen J, Vesala T, MacIntyre S, Ojala A (2014) Effects of cooling and internal wave motions on gas transfer coefficients in a boreal lake. Tellus 66B:22827. https://doi.org/10.3402/tellusb.v66.22827

Ikenaka Y, Eun H, Watanabe E, Kumon F, Miyabara Y (2005) Estimation of sources and inflow of dioxins and polycyclic aromatic hydrocarbons from the sediment core of Lake Suwa, Japan. Environ Pollut 138:529–537. https://doi.org/10.1016/j.envpol.2005.04.014

Imberger J (1985) The diurnal mixed layer. Limnol Oceanogr 30:737–770

Iwata H, Kosugi Y, Ono K, Mano M, Sakabe A, Miyata A, Takahashi K (2014) Cross-validation of open-path and closed-path eddy-covariance techniques for observing methane fluxes. Boundary-Layer Meteorol 151:95–118. https://doi.org/10.1007/s10546-013-9890-2

Jessup AT, Zappa CJ, Yeh H (1997) Defining and quantifying microscale wave breaking with infrared imagery. J Geophys Res 102:23,145–23,153

Joyce J, Jewell PW (2003) Physical controls on methane ebullition from reservoirs and lakes. Environ Eng Geosci 9:167–178

Katul G, Goltz SM, Hsieh C-I, Cheng Y, Mowry F, Sigmon J (1995) Estimation of surface heat and momentum fluxes using the flux-variance method above uniform and non-uniform terrain. Boundary-Layer Meteorol 74:237–260

Keller M, Stallard RF (1994) Methane emission by bubbling from Gatun Lake, Panama. J Geophys Res 99:8307–8319

Kimmel SJ, Wyngaard JC, Otte MJ (2002) "Log-chipper" turbulence in the convective boundary layer. J Atmos Sci 59:1124–1134

Kormann R, Meixner FX (2001) An analytical footprint model for non-neutral stratification. Boundary-Layer Meteorol 99:207–224

Kotthaus S, Grimmond CSB (2012) Identification of micro-scale anthropogenic CO_2, heat and moisture sources—processing eddy covariance fluxes for a dense urban environment. Atmos Environ 57:301–316. https://doi.org/10.1016/j.atmosenv.2012.04.024

Kumar P, Foufoula-Georgiou E (1994) Wavelet analysis in geophysics: an introduction. In: Foufoula-Georgiou E, Kumar P (eds) Wavelets in geophysics. Academic Press, New York, pp 1–43

Mahrt L (1998) Flux sampling errors for aircraft and towers. J Atmos Oceanic Technol 15:416–429

Martens CS, Klump JV (1980) Biogeochemical cycling in an organic-rich coastal marine basin—I. Methane sediment-water exchange processes. Geochim Cosmochim Acta 44:471–490

Mattson MD, Likens GE (1990) Air pressure and methane fluxes. Nature 347:718–719

McDermitt D, Burba G, Xu L, Anderson T, Komissarov A, Riensche B, Schedlbauer J, Starr G, Zona D, Oechel W, Oberbauer S, Hastings S (2011) A new low-power, open-path instrument for measuring methane flux by eddy covariance. Appl Phys B 102:391–405. https://doi.org/10.1007/s00340-010-4307-0

McGillis WR, Edson JB, Zappa CJ, Ware JD, McKenna SP, Terray EA, Hare JE, Fairall CW, Drennan W, Donelan M, DeGrandpre MD, Wanninkhof R, Reely RA (2004) Air-sea CO_2 exchange in the equatorial Pacific. J Geophys Res 109:C08S02

Nakamura H, Owa E (1952) On the "Kama-ana" (non-freezing parts in winter time) of the Suwa-Lake near Okaya-shi, Nagano Prefecture (in Japanese with English abstract). Bull Geol Surv Jpn 3:628–630

Park HD, Iwami C, Watanabe MF, Harada K, Okino T, Hayashi H (1998) Temporal variabilities of the concentrations of intra- and extracellular Microcystin and toxic Microcystis species in a hypertrophic lake, Lake Suwa, Japan (1991–1994). Environ Toxicol Water Qual 13:61–72

Percival DB, Walden AT (2000) Wavelet methods for time series analysis. Cambridge University Press, Cambridge

Podgrajsek E, Sahlée E, Bastviken D, Holst J, Lindroth A, Tranvik L, Rutgersson A (2014a) Comparison of floating chamber and eddy covariance measurements of lake greenhouse gas fluxes. Biogeosciences 11:4225–4233. https://doi.org/10.5194/bg-11-4225-2014

Podgrajsek E, Sahlée E, Rutgersson A (2014b) Diurnal cycle of lake methane flux. J Geophys Res Biogeosci 119:236–248. https://doi.org/10.1002/2013JG002327

Podgrajsek E, Sahlée E, Bastviken D, Natchimuthu S, Kljun N, Chmiel HE, Klemedtsson L, Rutgersson A (2016) Methane fluxes from a small boreal lake measured with the eddy covariance method. Limnol Oceanogr 61:S41–S50. https://doi.org/10.1002/lno.10245

Ripley B, Venables B, Bates DM, Hornik K, Gebhardt A, Firth D (2017) Package 'MASS'

Rousseeuw PJ, Leroy AM (2003) Robust regression and outlier detection. Wiley, New York

Saito M, Asanuma J, Miyata A (2007) Dual-scale transport of sensible and water vapor over a short canopy under unstable conditions. Water Resour Res 43:W05413

Scanlon TM, Albertson JD (2001) Turbulent transport of carbon dioxide and water vapor within a vegetation canopy during unstable conditions: identification of episodes using wavelet analysis. J Geophys Res 106:7251–7262

Scanlon TM, Sahu P (2008) On the correlation structure of water vapor and carbon dioxide in the atmospheric surface layer: a basis for flux partitioning. Water Resour Res 44:W10418. https://doi.org/10.1029/2008WR006932

Schaller C, Göckede M, Foken T (2017) Flux calculation of short turbulent events—comparison of three methods. Atmos Meas Tech 10:869–880

Schotanus P, Nieuwstadt FTM, de Bruin HAR (1983) Temperature measurement with a sonic anemometer and its application to heat and moisture fluxes. Boundary-Layer Meteorol 26:81–93

Schubert CJ, Diem T, Eugster W (2012) Methane emissions from a small wind shielded lake determined by eddy covariance, flux chambers, anchored funnels, and boundary model calculations: a comparison. Environ Sci Technol 46:4515–4522. https://doi.org/10.1021/es203465x

Sharma S, Magnuson JJ, Batt RD, Winslow LA, Korhonen J, Aono Y (2016) Direct observations of ice seasonality reveal changes in climate over the past 320–570 years. Sci Rep 6(25):061. https://doi.org/10.1038/srep25061

Tang J, Zhuang Q, Shannon RD, White JR (2010) Quantifying wetland methane emissions with process-based models of different complexities. Biogeosciences 7:3817–3837. https://doi.org/10.5194/bg-7-3817-2010

Thomas C, Martin JG, Goeckede M, Siqueira MB, Foken T, Law BE, Loescher HW, Katul G (2008) Estimating daytime subcanopy respiration from conditional sampling methods applied to multi-scalar high frequency turbulence time series. Agric For Meteorol 148:1210–1229. https://doi.org/10.1016/j.agrformet.2008.03.002

Tokida T, Miyazaki T, Mizoguchi M (2005) Ebullition of methane from peat with falling atmospheric pressure. Geophys Res Lett 32(L13):823. https://doi.org/10.1029/2005GL022949

van de Boer A, Moene AF, Graf A, Schüttemeyer D, Simmer C (2014) Detection of entrainment influences on surface-layer measurements and extension of Monin–Obukhov similarity theory. Boundary-Layer Meteorol 152:19–44

Varadharajan C, Hemond HF (2012) Time-series analysis of high-resolution ebullition fluxes from a stratified, freshwater lake. J Geophys Res 117(G02):004. https://doi.org/10.1029/2011JG001866

Vickers D, Mahrt L (1997) Quality control and flux sampling problems for tower and aircraft data. J Atmos Oceanic Technol 14:512–526

Walter KM, Smith LC, Chapin FS (2007) Methane bubbling from northern lakes: present and future contributions to the global methane budget. Philos Trans R Soc 365:1657–1676. https://doi.org/10.1098/rsta.2007.2036

Wanninkhof R (1992) Relationship between wind speed and gas exchange over the ocean. J Geophys Res 97:7373–7382

Wanninkhof R, Asher WE, Ho DT, Sweeney C, McGillis WR (2009) Advances in quantifying air-sea gas exchange and environmental forcing. Annu Rev Mar Sci 1:213–244. https://doi.org/10.1146/annurev.marine.010908.163742

Webb EK, Pearman GI, Leuning R (1980) Correction of flux measurements for density effects due to heat and water vapour transfer. Q J R Meteorol Soc 106:85–100

Wik M, Varner RK, Anthony KW, MacIntyre S, Bastviken D (2016) Climate-sensitive northern lakes and ponds are critical components of methane release. Nat Geosci 9:99–105. https://doi.org/10.1038/NGEO2578

Xu X, Riley WJ, Koven CD, Billesbach DP, Chang RYW, Commane R, Euskirchen ES, Hartery S, Harazono Y, Iwata H, McDonald KC, Miller CE, Oechel WC, Poulter B, Raz-Yaseef N, Sweeney C, Torn M, Wofsy SC, Zhang Z, Zona D (2016) A multi-scale comparison of modeled and observed seasonal methane emissions in northern wetlands. Biogeosciences 13:5043–5056. https://doi.org/10.5194/bg-13-5043-2016

Zappa CJ, Asher WE, Jessup AT (2001) Microscale wave breaking and air-water gas transfer. J Geophys Res 106:9385–9391